The Astrophysical Journal, 750:98 (12pp), 2012 May 10 doi:10.1088/0004-637X/750/2/98

THE INCIDENCE OF DEBRIS DISKS AT 24 μm AND 670 Myr

Laurie E. Urban[1,2], George Rieke[3], Kate Su[3], and David E. Trilling[1]
[1] Department of Physics and Astronomy, Northern Arizona University, P.O. Box 6010, Flagstaff, AZ 86011, USA
[2] Institute for Astronomy, University of Hawaii at Manoa, 2680 Woodlawn Drive, Honolulu, HI 96822, USA
[3] Steward Observatory, University of Arizona, Tucson, AZ 85721, USA
Received 2011 November 15; accepted 2012 February 29; published 2012 April 18

ABSTRACT

We use *Spitzer Space Telescope* 24 μm data to search for debris disks among 122 AFGKM stars from the ~670 Myr clusters Hyades, Coma Ber, and Praesepe, utilizing a number of advances in data reduction and determining the intrinsic colors of main-sequence stars. For our sample, the 1σ dispersion about the main-sequence $V-K_S$, K_S–[24] locus is approximately 3.1%. We identify seven debris disks at 10% or more ($\geqslant 3\sigma$ confidence level) above the expected K_S–[24] for purely photospheric emission. The incidence of excesses of 10% or greater in our sample at this age is $5.7^{+3.1}_{-1.7}$%. Combining with results from the literature, the rate is $7.8^{+4.2}_{-2.1}$% for early-type (B9–F4) stars and $2.7^{+3.3}_{-1.7}$% for solar-like (F5–K9) stars. Our primary sample has strict criteria for inclusion to allow comparison with other work; when we relax these criteria, three additional debris disks are detected. They are all around stars of solar-like type and hence reinforce our conclusion that disks around such stars are still relatively common at 670 Myr and are similar to the rate around early-type stars. The apparently small difference in decay rates between early-type and solar-like stars is inconsistent with the first-order theoretical predictions that the later type stellar disks would decay an order of magnitude more quickly than the earlier type ones.

Key words: circumstellar matter – infrared: stars – open clusters and associations: individual (Hyades, Coma Ber, Praesepe) – planetary systems

Online-only material: color figures

1. INTRODUCTION

Most stars form with an accompanying protoplanetary disk. Initially these disks begin as dense optically thick regions mostly made up of primordial gas and dust; these constituents make the disks readily detectable in thermal continuum and multiple emission lines. These disks provide the environment for massive planet formation. Ironically, once planets have formed, the disks disappear after a few million years (e.g., Haisch et al. 2001). The resulting planetary systems remain difficult to detect directly. The systems have not ceased evolving at this point; terrestrial planets continue to grow from the solid remnants of the disks (e.g., Agnor et al. 1999; Chambers 2001; Raymond et al. 2006; Morishima et al. 2010), and massive planets may migrate inward or outward (Hahn & Malhotra 1999; Gomes et al. 2004; Levison et al. 2007). These processes are marked by dynamical stirring of the asteroidal or planetesimal bodies, which are pulverized into dust that is warmed by the star and glows in the infrared. This dust dissipates rapidly due to radiation pressure, Poynting–Robertson drag, or collisional destruction (e.g., Lagrange et al. 2000; Dominik & Decin 2003). Hence, these debris disks must reflect the current state of the systems, and the infrared excesses provide snapshots of the state of the circumstellar material and of the degree of dynamical activity causing it to undergo collisions. A series of these snapshots gives a view of evolution of the planetary system (e.g., Kenyon & Bromley 2004; Wyatt 2008).

Debris disks were first observed in the infrared with the *Infrared Astronomical Satellite* (Aumann et al. 1984; see also Rhee et al. 2007). Many subsequent debris disk observations were made with the *Infrared Space Observatory* (e.g., Decin et al. 2000, 2003; Spangler et al. 2001; Habing et al. 2001). The Multiband Imaging Photometer for *Spitzer* (MIPS; Rieke et al. 2004) on board the *Spitzer Space Telescope* provided another significant increase in sensitivity, observing a large number of debris disks at 24 and 70 μm. *Herschel* is currently extending our understanding of large samples of debris disks to longer infrared and submillimeter wavelengths.

The evolution of the 24 μm emission of debris disks is particularly interesting because this wavelength traces inner zones of these systems that may reveal processes near the ice line (Morales et al. 2011) and because the dynamical timescale for these zones is shorter than for those probed at longer wavelengths, so the evolution should proceed relatively rapidly. Previous surveys have verified that the 24 μm emission of debris disks decays significantly over time. About 50% of early-type stars younger than 30 Myr have debris disks detected at 24 μm (Rieke et al. 2005; Su et al. 2006). However, at 100–115 Myr the detection rate has dropped to about 35% (see below). Gáspár et al. (2009) find the Praesepe cluster at ~750 Myr to have an excess rate of only ~2%. Surveys of stars older than ~1 Gyr report an excess rate of ~4% or less (Meyer et al. 2008; Trilling et al. 2008; Koerner et al. 2010).

A better understanding of the decay process will help build a picture of the evolution of planetary systems. Toward this goal, we examine MIPS data at 24 μm for three stellar clusters with ages ~670 Myr: Hyades (~650 Myr; Perryman et al. 1998; De Gennaro et al. 2009), Coma Ber (~600 Myr; Collier et al. 2009), and Praesepe (~750 Myr; Gáspár et al. 2009). We improve on previous studies by combining results for three separate clusters of similar ages. This study also improves over similar work on field stars because the ages of our sample are much better constrained. Combining three clusters provides a high-fidelity measurement over a large range of spectral types from early K for the closest cluster (Hyades) to A-types with reasonable statistics for the richest but most distant (Praesepe).

We discuss in Section 2 how we selected our sample for this study, reduced the data, excluded stars with large errors or bad

measurements, and placed our retained targets on a $V-K_S$ versus K_S–[24] color–color diagram (Gorlova et al. 2006). We improve on previous results by utilizing a new locus for the photospheres of main-sequence stars. In Section 3 we determine which stars have excess emission at 24 μm and compare our work with that of others. Section 4 discusses the excess rate at 670 Myr as a function of spectral type. We also compare these results to previously published excess rates and discuss the decay rate of 24 μm excesses. Our conclusions are in Section 5.

2. OBSERVATIONS AND DATA REDUCTION

2.1. Sample Selection and Data Reduction

We searched the *Spitzer* archive for observations of stars in published membership lists for the Hyades, Coma Ber, and Praesepe. Our initial samples included 78 stars from the Hyades (Paulson et al. 2004), 84 from Coma Ber (Abad & Vicente 1999), and 193 from Praesepe (Gáspár et al. 2009). Some of the stars have accompanying 70 μm observations; here we only report the 24 μm results, some of which have been published previously (Rieke et al. 2005; Su et al. 2006; Cieza et al. 2008; Carpenter et al. 2008; Gáspár et al. 2009).

For consistency, we re-processed all the data as part of a *Spitzer* legacy catalog (Su et al. 2010), using the MIPS instrument team Data Analysis Tool (Gordon et al. 2005) for basic reduction. In addition, a second flat field constructed from the 24 μm data itself was applied to all the 24 μm results to remove scattered-light gradients and dark latency (e.g., Engelbracht et al. 2007). The processed data were then combined using the World Coordinate System information to produce final mosaics with pixels half the size of the physical pixel scale. The majority of the stars in the Praesepe cluster were observed in scan-map mode as presented in Gáspár et al. (2009). We used the same data reduction as in that paper but did the photometry differently, as described below.

We extracted the photometry using point-spread function (PSF) fitting. The input PSFs were constructed using observed calibration stars and smoothed STinyTim model PSFs and have been tested to ensure that the photometry results are consistent with the MIPS calibration (Engelbracht et al. 2007). Aperture photometry was also performed, but the results were only used as a reference to screen targets that might have contamination from nearby sources or background nebulosity.

The random photometry errors were estimated based on the pixel-to-pixel variation within a $2' \times 2'$ box centered on the source position. The final photometry errors also included the errors from the detector repeatability ($\lesssim$1% at 24 μm; Engelbracht et al. 2007). The measured flux densities, 24 μm magnitudes ([24], using 7.17 Jy as the zero magnitude flux; Rieke et al. 2008), and associated errors are listed in Table 1.

2.2. Culling the Sample

We further trimmed the sample based on the criteria described below to ensure that our analysis only includes measurements of uniform quality. Because of *Spitzer*'s exceptional pointing accuracy ($<1''$), we considered a source only where the PSF fitting position falls within $1''.5$ of the member position (from the membership catalogs). Sources that failed this positional test are noted as "6" in Table 1. We then eliminated by visual inspection of the 24 μm images all stars with a nearby source (within $6''$) of the target star (noted as "1" in Table 1). We excluded all stars that are classified as giants (luminosity class III) (noted as "7" in Table 1). We also excluded all stars that could not be detected by eye, implying a signal-to-noise ratio <3 (noted as "3" in Table 1); this step guarded against false detections in regions where the background had residual structure. Finally, we excluded all measurements with an FWHM either much greater or less than the nominal FWHM of the MIPS beam of $\sim 5''.5$ (noted as "2" in Table 1), which is an indication of confusion with a second object.

In our analysis we rely on K_S magnitudes from Two Micron All Sky Survey (2MASS; Cutri et al. 2003). For stars in the *Hipparcos* catalog (Perryman et al. 1997), we adopted the listed Johnson V photometry. For stars that are not in *Hipparcos* but are in Praesepe we adopted the V magnitudes gathered by Gáspár et al. (2009); we collected additional V magnitudes from the SIMBAD database. A total of eight stars have no available V magnitudes, noted as "5" in Table 1; these stars are not included in our analysis.

Finally, we removed stars with large errors in K_S–[24]. (The errors from $V-K_S$ are not used to remove stars from our sample since the errors in the V magnitudes are generally small and any stars with large errors in K_S will be eliminated because of the errors in K_S–[24].) We took the K_S errors (e_{K_S}) from 2MASS. For the MIPS photometry, we combined two types of error. The first, $e_{24,\mathrm{pp}}$, is based on the pixel-to-pixel variation near the source and represents the random photometric error. The second arises from the overall repeatability of the MIPS 24 μm measurement at $\sim$1% of the source fluxes (Engelbracht et al. 2007). The final error (e_{24}) in the 24 μm flux (f_{24}) is thus

$$e_{24} = \sqrt{e_{24,\mathrm{pp}}^2 + (0.01 * f_{24})^2}. \quad (1)$$

We combine the 24 μm errors with the K_S errors to find the total (rms) error on K_S–[24]. Only stars with $e_{K_S-[24]} < 0.05$ were retained (exclusion note "4" in Table 1). Our final sample contains 122 stars: 61 from Hyades, 25 from Coma Ber, and 36 from Praesepe. We present all 355 stars in Table 1, where we indicate the 122 stars included and the reason the remaining were excluded from analysis.

2.3. Main-sequence Definition and Scatter

Figure 1 shows the $V-K_S$ versus $K_S - [24]$ color–color plot for the whole sample and the final sample retained in our analysis. Gorlova et al. (2006) introduced such a diagram to determine the photospheric locus for main-sequence stars in the Pleaides cluster. They identified stars with infrared excesses as those with K_S–[24] positive by more than 3σ relative to the photospheric locus. Here we apply the same general technique. We have used a sample of $\sim$1300 stars from the *Spitzer* archive (Su et al. 2010) to derive the locus of main-sequence stars in $V-K_S$, K_S–[24] space. We define $x = V-K_S - 0.8$. For $x \leqslant 0$, we find the following empirical fits:

$$K_S\text{–}[24] = \frac{(50 + 661x + 282x^2 + 653x^3)}{10{,}000}; \quad (2)$$

whereas for $x > 0$, we find

$$K_{S-[24]} = \frac{(55-134x+655.5x^2-1095x^3+664.15x^4-145.8x^5+11.01x^6-0.03x^7}{10{,}000}. \quad (3)$$

At the juncture where $V-K_S = 0$ the equations agree so either of them applies. The rms scatter around these fits (determined by fitting Gaussians to the distribution so the result is not biased by stars with excesses) is 0.038 mag.

Table 1
Cluster Stars Considered

Name	Sp Type	V	K_S	$K_{\rm err}$	$f24$	[24]	$[24]_{\rm err}$	$(K–[24])_{\rm err}$	Incl?	Excl. Note	Cluster
Cl* Melotte 111 AV 1119	G5V	10.830	9.295	0.019	1.453	9.233	0.057	0.060	n	4	c
Cl* Melotte 111 AV 1183	K3V	11.500	8.972	0.020	1.932	8.924	0.043	0.047	y	...	c
Cl* Melotte 111 AV 1280	K4V:	11.720	9.476	0.018	1.164	9.474	0.068	0.070	n	1,2,4	c
Cl* Melotte 111 AV 1284	F2	4.780	3.236	0.244	395.500	3.146	0.011	0.244	n	4	c
Cl* Melotte 111 AV 1288	G0	12.520	10.519	0.019	...	...	0.011	0.022	n	3	c
Cl* Melotte 111 AV 1292	F8V	10.990	9.606	0.021	1.047	9.589	0.077	0.080	n	4	c
Cl* Melotte 111 AV 1293	G5V:	12.580	10.796	0.024	0.359	10.750	0.132	0.135	n	4	c
Cl* Melotte 111 AV 1297	G8V	10.440	8.752	0.021	2.418	8.680	0.070	0.073	n	4	c
Cl* Melotte 111 AV 1420	K2V:	11.220	9.078	0.020	1.768	9.020	0.044	0.048	y	...	c
Cl* Melotte 111 AV 1435	K2V:	11.490	9.424	0.018	1.214	9.428	0.066	0.068	n	1,4	c
Cl* Melotte 111 AV 1464	...	11.430	9.417	0.025	1.190	9.450	0.148	0.150	n	2,4	c
Cl* Melotte 111 AV 1487	K0V:	...	10.813	0.018	0.348	10.784	0.132	0.133	n	4,5	c
Cl* Melotte 111 AV 1537	G5V:	11.300	9.844	0.024	0.814	9.862	0.094	0.097	n	4	c
Cl* Melotte 111 AV 1548	G8V:	12.720	10.722	0.022	0.371	10.714	0.124	0.126	n	1,2,4	c
Cl* Melotte 111 AV 1561	G5V:	11.560	10.023	0.024	0.712	10.008	0.112	0.115	n	4	c
Cl* Melotte 111 AV 1584	G0V:	12.010	10.416	0.021	0.462	10.478	0.123	0.125	n	1,4	c
Cl* Melotte 111 AV 1623	K2V:	12.530	10.270	0.021	0.586	10.219	0.131	0.132	n	1,4	c
Cl* Melotte 111 AV 1695	G0V:	11.790	10.315	0.021	0.647	10.111	0.120	0.121	n	4	c
Cl* Melotte 111 AV 1711	G8V:	11.880	9.970	0.021	0.811	9.867	0.094	0.096	n	4	c
Cl* Melotte 111 AV 1768	G5V:	12.130	10.568	0.021	0.427	10.563	0.111	0.113	n	4	c
Cl* Melotte 111 AV 190	...	...	9.224	0.018	1.453	9.233	0.122	0.123	n	4,5	c
Cl* Melotte 111 AV 1966	G5V:	12.520	10.848	0.023	0.462	10.478	0.111	0.113	n	1,4	c
Cl* Melotte 111 AV 2049	G8V:	12.200	10.637	0.021	0.500	10.391	0.101	0.103	n	1,2,4	c
Cl* Melotte 111 AV 2062	K0V:	11.320	8.995	0.019	1.823	8.987	0.045	0.049	y	...	c
Cl* Melotte 111 AV 2331	G7V	11.890	10.205	0.021	0.618	10.161	0.130	0.132	n	2,4	c
Cl* Melotte 111 AV 472	...	12.840	10.895	0.017	0.331	10.839	0.153	0.154	n	4	c
Cl* Melotte 111 AV 477	G5V:	12.070	10.518	0.017	0.444	10.521	0.114	0.115	n	4	c
Cl* Melotte 111 AV 481	G0V:	12.230	10.511	0.016	0.489	10.416	0.112	0.113	n	1,2,4	c
Cl* Melotte 111 AV 484	F5	11.970	10.826	0.017	0.269	11.065	0.189	0.190	n	1,2,4	c
Cl* Melotte 111 AV 497	G0V:	12.430	10.840	0.019	0.312	10.903	0.161	0.163	n	4	c
Cl* Melotte 111 AV 501	G8V:	12.660	10.766	0.019	0.399	10.636	0.122	0.124	n	2,4	c
Cl* Melotte 111 AV 519	G5V:	11.910	9.630	0.016	1.212	9.430	0.067	0.069	n	4	c
Cl* Melotte 111 AV 551	G0V:	11.850	10.531	0.018	0.483	10.430	0.109	0.110	n	1,2,4	c
Cl* Melotte 111 AV 569	G0V:	12.510	10.741	0.019	0.410	10.606	0.115	0.117	n	4	c
Cl* Melotte 111 AV 571	G0V:	12.630	10.424	0.018	0.419	10.583	0.143	0.144	n	2,4	c
Cl* Melotte 111 AV 573	K0V:	11.480	9.415	0.018	1.496	9.201	0.054	0.057	n	4	c
Cl* Melotte 111 AV 605	G0V:	11.090	9.717	0.017	0.895	9.760	0.092	0.094	n	4	c
Cl* Melotte 111 AV 610	K4V:	10.940	7.542	0.020	7.923	7.392	0.024	0.031	y	...	c
Cl* Melotte 111 AV 669	G0V:	11.420	9.813	0.016	0.832	9.838	0.097	0.099	n	4	c
Cl* Melotte 111 AV 726	G0V:	11.220	9.671	0.018	0.926	9.722	0.092	0.093	n	1,2,4	c
Cl* Melotte 111 AV 773	K0V:	11.200	9.332	0.020	1.261	9.387	0.062	0.065	n	1,2,4	c
Cl* Melotte 111 AV 838	G5V:	11.940	10.328	0.018	0.477	10.443	0.126	0.127	n	2,4	c
Cl* Melotte 111 AV 967	...	...	11.646	0.021	0.270	11.059	0.206	0.207	n	2,4,5	c
BD+25 2478	A0V	10.640	10.629	0.014	0.593	10.207	0.087	0.088	n	1,2,4	c
BD+25 2485	G7V	9.400	7.165	0.020	9.724	7.169	0.020	0.029	y	...	c
BD+25 2509	G8V	11.340	9.208	0.019	1.557	9.158	0.054	0.057	n	4	c
BD+26 2303	F8V	10.050	8.802	0.017	2.134	8.816	0.082	0.083	n	4	c
BD+26 2310	G5V	10.980	9.389	0.018	1.231	9.413	0.070	0.072	n	4	c
BD+26 2312	K1V	9.560	6.104	0.016	28.860	5.988	0.012	0.020	y	...	c
BD+26 2333	F8V	10.360	8.793	0.024	2.086	8.841	0.081	0.084	n	4	c
BD+26 2336	F3V	9.570	8.456	0.019	2.984	8.452	0.062	0.065	n	1,4	c
BD+26 2339	F5V	10.040	8.903	0.022	1.730	9.044	0.102	0.105	n	2,4	c
BD+26 2342	K0V	10.470	8.611	0.021	2.248	8.759	0.077	0.080	n	2,4	c
BD+28 2091	F8V	10.020	8.750	0.021	2.230	8.768	0.079	0.081	n	1,4	c
GJ 9410	K4V	11.090	8.146	0.023	4.264	8.064	0.039	0.045	y	...	c
GSC 01988-00346	G5V:	11.940	10.171	0.018	0.679	10.059	0.115	0.116	n	2,4	c
GSC 01991-00357	G5V:	11.850	10.339	0.018	0.277	11.032	0.201	0.201	n	1,2,4	c
GSC 01991-00612	G5V:	12.660	10.796	0.018	0.336	10.823	0.137	0.138	n	1,2,4	c
GSC 01991-00727	G0V:	11.560	10.068	0.028	0.735	9.973	0.108	0.111	n	4	c
HD 105371	F6V	8.500	7.292	0.024	8.128	7.364	0.024	0.034	y	...	c
HD 105805	A4Vn	6.010	5.600	0.033	38.720	5.669	0.012	0.035	y	...	c
HD 105898	G2V	7.510	5.307	0.017	55.610	5.276	0.011	0.020	y	...	c
HD 106293	F5V	8.080	6.990	0.033	11.320	7.004	0.019	0.038	y	...	c
HD 106691	F5IV	8.090	7.036	0.017	10.550	7.081	0.020	0.026	y	...	c
HD 106857	F5V	8.960	7.726	0.018	5.988	7.696	0.030	0.035	n	1	c

Table 1
(Continued)

Name	Sp Type	V	K_S	$K_{\rm err}$	$f24$	[24]	$[24]_{\rm err}$	$(K–[24])_{\rm err}$	Incl?	Excl. Note	Cluster
HD 106946	F2V	7.850	6.928	0.017	12.110	6.931	0.018	0.025	y	...	c
HD 106947	F7V	8.690	7.371	0.021	7.466	7.456	0.026	0.033	y	...	c
HD 107086	F8V	7.560	6.474	0.031	17.760	6.515	0.014	0.034	y	...	c
HD 107159	A5V	7.770	7.006	0.029	11.410	6.996	0.019	0.035	y	...	c
HD 107214	G0V	9.020	7.492	0.027	7.086	7.513	0.027	0.038	y	...	c
HD 107427	A3V	9.060	8.746	0.018	2.150	8.808	0.080	0.082	n	1,2,4	c
HD 107611	F6V	8.510	7.325	0.020	8.409	7.327	0.022	0.030	n	1	c
HD 107655	A0V	6.210	6.167	0.024	22.640	6.252	0.013	0.027	y	...	c
HD 107701	F7V	8.550	7.024	0.018	11.210	7.015	0.020	0.027	y	...	c
HD 107793	F8V	9.100	7.685	0.023	6.434	7.618	0.029	0.037	n	1	c
HD 108007	A7V+...	6.410	5.731	0.016	33.560	5.824	0.012	0.020	n	2	c
HD 108382	A4V	4.980	4.649	0.024	118.800	4.452	0.011	0.026	y	...	c
HD 108945	A2pv	5.470	5.269	0.017	55.360	5.281	0.011	0.020	n	1	c
HD 108956	F8V	7.120	5.609	0.026	41.730	5.588	0.012	0.028	y	...	c
HD 108976	F6V	8.560	7.404	0.018	7.845	7.402	0.024	0.030	y	...	c
HD 109127	F3V	9.070	8.236	0.017	3.540	8.266	0.051	0.054	n	2,4	c
HD 109306	F3V	8.610	7.702	0.016	6.165	7.664	0.029	0.033	y	...	c
HD 109307	A4Vm	6.280	5.989	0.026	27.130	6.055	0.013	0.029	y	...	c
HD 116706	A3IV	5.750	5.502	0.018	42.310	5.573	0.012	0.021	y	...	c
HD 018632	G5	7.970	5.841	0.024	34.390	5.798	0.012	0.027	y	...	h
HD 020430	F8V	7.380	5.992	0.021	28.180	6.014	0.012	0.024	n	2	h
HD 025825	G0	7.850	6.446	0.024	18.890	6.448	0.015	0.029	y	...	h
HD 026767	G0	8.050	6.534	0.017	17.570	6.527	0.016	0.023	y	...	h
HD 026784	F8V	7.110	5.862	0.017	34.900	5.782	0.012	0.021	y	...	h
HD 027250	G5	8.620	6.921	0.016	12.320	6.912	0.021	0.026	n	1	h
HD 027282	G8V	8.470	6.787	0.016	13.800	6.789	0.019	0.024	y	...	h
HD 027406	G0V	7.460	6.124	0.018	26.200	6.093	0.014	0.023	y	...	h
HD 027628	A3m	5.720	4.960	0.017	73.770	4.969	0.011	0.020	y	...	h
HD 027685	G4V	7.860	6.203	0.018	23.970	6.190	0.012	0.022	y	...	h
HD 027732	G5	8.840	7.121	0.016	10.350	7.101	0.023	0.028	y	...	h
HD 027749	A1m	5.640	4.945	0.021	72.680	4.985	0.011	0.024	y	...	h
HD 027771	G5	9.110	7.145	0.017	9.956	7.144	0.024	0.030	y	...	h
HD 027808	F8V	7.130	5.871	0.020	31.180	5.904	0.013	0.024	y	...	h
HD 027835	G2V	8.203	6.797	0.026	13.520	6.811	0.015	0.030	y	...	h
HD 027859	G2V	7.790	6.290	0.016	22.450	6.261	0.013	0.020	y	...	h
HD 027962	A2IV	4.300	4.098	0.029	151.700	4.186	0.011	0.031	y	...	h
HD 027990	K2V	8.990	6.767	0.021	14.200	6.758	0.015	0.026	y	...	h
HD 028068	G1V	8.040	6.436	0.027	20.060	6.383	0.013	0.030	y	...	h
HD 028099	G2V	8.100	6.547	0.021	16.660	6.585	0.014	0.025	y	...	h
HD 028205	G0	7.410	6.141	0.024	24.500	6.166	0.014	0.028	y	...	h
HD 028226	Am	5.720	5.055	0.018	74.370	4.960	0.011	0.021	y	...	h
HD 028237	F8	7.490	6.158	0.017	24.230	6.178	0.012	0.021	n	1	h
HD 028258	G5	9.020	7.003	0.021	12.060	6.935	0.020	0.029	y	...	h
HD 028344	G2V	7.830	6.404	0.020	20.130	6.379	0.013	0.024	y	...	h
HD 028355	A7V	5.020	4.534	0.033	138.300	4.287	0.011	0.035	y	...	h
HD 028462	K1V	9.080	7.139	0.024	10.290	7.108	0.017	0.030	y	...	h
HD 028527	A6IV	4.780	4.364	0.036	122.800	4.416	0.011	0.038	y	...	h
HD 028546	Am	5.470	4.903	0.023	75.950	4.937	0.011	0.026	y	...	h
HD 028593	G5	8.590	6.884	0.023	12.530	6.894	0.020	0.030	y	...	h
HD 028635	F8	7.780	6.455	0.021	18.640	6.463	0.013	0.025	y	...	h
HD 028783	K0	8.929	6.770	0.016	14.860	6.709	0.014	0.022	n	2	h
HD 028805	G5	8.641	6.941	0.026	11.920	6.948	0.016	0.031	y	...	h
HD 028878	G5	9.357	7.351	0.024	8.431	7.324	0.020	0.031	y	...	h
HD 028977	K0	9.644	7.553	0.026	7.076	7.514	0.024	0.035	y	...	h
HD 028992	F8	7.900	6.445	0.026	18.940	6.445	0.014	0.029	y	...	h
HD 029159	K0	9.345	7.373	0.015	8.087	7.369	0.021	0.026	y	...	h
HD 029388	A6V	4.270	4.105	0.334	187.200	3.958	0.011	0.334	n	4	h
HD 029461	G5	7.960	6.443	0.021	19.370	6.421	0.013	0.025	y	...	h
HD 029488	A5Vn	4.670	4.229	0.036	145.400	4.232	0.011	0.038	y	...	h
HD 030210	Am	5.350	4.974	0.020	70.940	5.012	0.011	0.023	y	...	h
HD 030246	G5	8.300	6.738	0.033	14.070	6.768	0.015	0.036	y	...	h
HD 030505	F5	8.980	7.059	0.026	11.000	7.035	0.017	0.031	y	...	h
HD 030589	F8	7.720	6.355	0.016	19.960	6.388	0.015	0.022	y	...	h
HD 030809	F8	7.900	6.671	0.021	15.820	6.641	0.017	0.027	y	...	h
HD 031609	G5	8.890	7.235	0.017	9.617	7.181	0.023	0.029	y	...	h

Table 1
(Continued)

Name	Sp Type	V	K_S	$K_{\rm err}$	$f24$	[24]	$[24]_{\rm err}$	$(K–[24])_{\rm err}$	Incl?	Excl. Note	Cluster
HD 032347	K0	9.000	7.226	0.027	9.029	7.250	0.024	0.036	n	2	h
HD 033254	A2m	5.430	4.861	0.023	77.810	4.911	0.011	0.026	y	...	h
HD 240648	K0	8.820	7.128	0.017	9.941	7.145	0.023	0.028	y	...	h
HD 242780	K0	9.030	7.302	0.021	8.794	7.278	0.027	0.034	n	2	h
HD 283704	G5	9.190	7.462	0.029	7.711	7.421	0.029	0.041	y	...	h
HD 284552	K0	10.690	7.686	0.026	6.528	7.602	0.033	0.042	n	1	h
HD 284653	K2V	10.690	7.995	0.033	4.578	7.987	0.034	0.047	y	...	h
HD 284930	K0	10.290	7.742	0.020	5.629	7.763	0.028	0.034	n	2	h
HD 285252	K2	8.990	6.910	0.021	11.980	6.943	0.020	0.029	y	...	h
HD 285367	K2	9.310	7.254	0.023	9.446	7.201	0.019	0.030	y	...	h
HD 285690	K0	9.570	7.322	0.017	9.825	7.158	0.024	0.029	y	...	h
HD 285773	G5	8.950	7.055	0.027	10.890	7.046	0.017	0.032	y	...	h
HD 285830	K0	9.480	7.348	0.020	8.338	7.336	0.026	0.033	y	...	h
HD 285876	K0	11.020	7.895	0.024	5.171	7.855	0.032	0.040	n	1	h
HD 285931	K1	8.480	6.465	0.024	18.660	6.462	0.013	0.027	y	...	h
HD 286363	M0	10.120	7.574	0.021	6.906	7.541	0.022	0.031	y	...	h
HD 286554	M0V	11.280	8.046	0.027	4.939	7.905	0.045	0.052	n	...	h
HD 286734	K5.5	10.890	7.786	0.021	6.130	7.670	0.036	0.042	y	...	h
HD 286789	K7	10.480	7.795	0.031	6.312	7.638	0.026	0.040	y	...	h
HD 286929	K5	10.040	7.480	0.023	7.508	7.450	0.029	0.037	n	1,2	h
HIP 13600	K0	8.830	7.179	0.024	9.780	7.163	0.023	0.033	y	...	h
HIP 13806	G5	8.920	6.905	0.023	12.350	6.910	0.018	0.029	y	...	h
HIP 15563	M0	9.650	6.881	0.023	13.320	6.828	0.018	0.029	y	...	h
HIP 16529	G5	8.880	6.907	0.016	12.230	6.920	0.019	0.025	y	...	h
HIP 17766	M1V	10.850	7.509	0.016	7.734	7.418	0.026	0.030	n	2	h
HIP 18018	K7	10.170	7.395	0.020	8.108	7.367	0.027	0.033	n	2	h
HIP 18946	K5	10.120	7.600	0.020	6.963	7.532	0.024	0.031	n	2	h
HIP 19082	...	11.410	8.107	0.026	4.473	8.012	0.036	0.044	n	1	h
HIP 19441	K5V	10.100	7.264	0.020	9.812	7.159	0.023	0.031	n	2	h
HIP 21179	K0	11.000	7.654	0.020	8.313	7.339	0.014	0.024	y	...	h
HIP 22177	K4.5	10.920	7.826	0.020	5.617	7.765	0.025	0.032	y	...	h
HIP 23312	K2	9.710	7.589	0.026	6.553	7.598	0.022	0.034	y	...	h
2MASS J08362985+1857570	F6V	9.409	8.300	0.021	3.599	8.248	0.070	0.073	n	4	p
2MASS J08364896+1915265	G4V	11.180	9.690	0.022	...	...	...	...	n	2,4,6	p
2MASS J08370203+1936171	F6V	9.182	8.060	0.020	4.249	8.068	0.056	0.059	n	4	p
2MASS J08371635+1929103	K6V	99.990	10.470	0.019	0.547	10.293	0.306	0.306	n	2,4	p
2MASS J08371829+1941564	G5V	11.440	9.800	0.019	0.937	9.709	0.182	0.183	n	2,4	p
2MASS J08372638+1929128	K5V	...	10.830	0.019	...	...	...	...	n	2,4,5,6	p
2MASS J08372755+1937033	G8V	11.650	9.810	0.018	0.846	9.820	0.183	0.184	n	2,4	p
2MASS J08372793+1933451	F6V	9.790	8.460	0.020	2.754	8.539	0.052	0.056	n	4	p
2MASS J08372819+1909443	F6V	9.500	8.400	0.021	3.043	8.430	0.050	0.055	n	4	p
2MASS J08373381+2000492	F0Vn	8.698	7.950	0.033	4.770	7.942	0.046	0.057	n	4	p
2MASS J08373624+1915542	...	13.470	10.760	0.022	...	...	...	...	n	3,4	p
2MASS J08373699+1943585	Am	7.771	7.290	0.020	8.247	7.348	0.024	0.031	y	...	p
2MASS J08374070+1931063	F0Vn	8.240	7.660	0.018	6.060	7.683	0.030	0.035	y	...	p
2MASS J08374235+1908015	F4V	9.870	8.580	0.020	2.603	8.600	0.054	0.057	n	4	p
2MASS J08374640+1935575	...	12.330	10.240	0.018	...	...	...	...	n	2,4	p
2MASS J08374660+1926181	G0	10.660	9.280	0.024	1.352	9.311	0.113	0.115	n	4	p
2MASS J08374675+1916020	A5V	6.720	6.170	0.018	24.711	6.157	0.017	0.024	y	...	p
2MASS J08374739+1906247	...	12.280	10.200	0.018	...	...	...	...	n	2,4,6	p
2MASS J08374998+1953287	G	11.410	9.330	0.020	1.555	9.160	0.108	0.110	n	2,4	p
2MASS J08375208+1959138	G5V	11.260	9.690	0.020	1.018	9.619	0.146	0.148	n	2,4	p
2MASS J08375703+1914103	G8V	11.810	10.040	0.020	0.720	9.996	0.209	0.210	n	4	p
2MASS J08380758+1959163	...	12.110	9.900	0.020	0.758	9.939	0.199	0.200	n	4	p
2MASS J08380808+2026223	...	11.720	9.930	0.019	...	...	...	...	n	3,4,6	p
2MASS J08381421+1947234	...	...	10.910	0.036	...	...	...	...	n	2,4,5,6	p
2MASS J08381427+1921552	G5V	10.900	9.190	0.020	1.578	9.143	0.094	0.096	n	4	p
2MASS J08382311+2012263	...	7.830	6.650	0.016	15.473	6.665	0.019	0.024	y	...	p
2MASS J08382429+2006217	G0V	10.550	9.180	0.018	1.493	9.204	0.106	0.108	n	4	p
2MASS J08382963+1951450	...	14.010	10.930	0.019	...	...	...	...	n	3,4	p
2MASS J08383216+1927548	...	10.010	7.540	0.016	7.341	7.474	0.026	0.030	y	...	p
2MASS J08383425+1951369	K0III	9.160	6.690	0.018	14.931	6.704	0.019	0.026	n	7	p
2MASS J08383723+1901161	K5V	...	10.610	0.016	...	...	...	...	n	2,4,5,6	p
2MASS J08383776+1938480	F6V	10.560	9.220	0.020	1.452	9.234	0.106	0.107	n	2,4	p
2MASS J08383786+1959231	F0V	8.150	7.610	0.018	6.160	7.665	0.029	0.034	y	...	p

Table 1
(Continued)

Name	Sp Type	V	K_S	$K_{\rm err}$	$f24$	[24]	$[24]_{\rm err}$	$(K–[24])_{\rm err}$	Incl?	Excl. Note	Cluster
2MASS J08384695+1930033	F4V	9.000	8.220	0.020	4.013	8.130	0.041	0.045	y	...	p
2MASS J08385001+2004035	G0	10.800	9.370	0.018	1.237	9.408	0.117	0.118	n	2,4	p
2MASS J08385354+1934170	K6V	14.070	10.960	0.022	...	...	...	...	n	3,4,6	p
2MASS J08385506+1911539	K3V	10.140	8.040	0.018	4.873	7.919	0.035	0.040	y	...	p
2MASS J08390185+2000194	K5V	11.880	9.070	0.018	1.788	9.008	0.084	0.086	n	2,4	p
2MASS J08390228+1919343	K	12.390	10.260	0.019	0.632	10.137	0.247	0.247	n	3,4	p
2MASS J08390283+1943289	F7V	9.299	8.120	0.021	4.287	8.058	0.040	0.045	y	...	p
2MASS J08390321+2002376	...	14.410	11.050	0.020	...	...	...	...	n	3,4,6	p
2MASS J08390359+1959591	A9V	8.315	7.770	0.018	5.758	7.738	0.030	0.035	y	...	p
2MASS J08390411+1931216	K5V	13.750	10.860	0.016	...	...	...	...	n	3	p
2MASS J08390523+2007018	F5V	9.383	8.410	0.027	3.101	8.410	0.050	0.056	n	4	p
2MASS J08390612+1940364	A9Vn	7.446	6.710	0.018	14.274	6.752	0.018	0.026	y	...	p
2MASS J08390649+1900360	...	...	11.300	0.022	...	...	...	...	n	3,4,5,6	p
2MASS J08390909+1935327	A9V	8.500	7.880	0.026	4.964	7.899	0.036	0.045	y	...	p
2MASS J08391014+1940423	F6	9.408	8.410	0.016	2.914	8.477	0.053	0.056	n	4	p
2MASS J08391217+1906561	...	10.580	9.260	0.018	1.497	9.201	0.106	0.108	n	4	p
2MASS J08391499+2012388	G5V	11.310	9.650	0.020	0.955	9.689	0.193	0.194	n	2,4	p
2MASS J08391972+2003107	K0V	9.220	7.080	0.021	10.649	7.071	0.021	0.029	y	...	p
2MASS J08392185+1951402	...	12.530	10.370	0.020	0.597	10.200	0.267	0.268	n	2,4	p
2MASS J08392498+1927336	F7V	10.470	9.000	0.018	1.967	8.904	0.073	0.075	n	4	p
2MASS J08392858+1928251	K	11.630	9.530	0.021	1.186	9.454	0.123	0.125	n	4	p
2MASS J08392940+1947118	...	12.640	10.060	0.018	0.655	10.098	0.328	0.329	n	3,4	p
2MASS J08393042+2004087	F8V	10.320	8.810	0.018	2.163	8.801	0.068	0.071	n	4	p
2MASS J08393342+2010102	K2V	9.064	6.130	0.021	27.606	6.036	0.017	0.027	y	...	p
2MASS J08393643+1915378	K7V	14.380	11.010	0.018	...	...	...	...	n	3,4	p
2MASS J08393836+1926272	K3	12.630	10.290	0.020	...	...	...	...	n	3,4,6	p
2MASS J08394265+1946425	F0III	6.650	6.000	0.018	28.102	6.017	0.016	0.024	n	7	p
2MASS J08394279+2005103	A5V	7.728	7.160	0.020	9.327	7.214	0.022	0.030	y	...	p
2MASS J08394333+1925121	K5V	11.410	7.900	0.023	...	...	...	...	n	4,6	p
2MASS J08394466+1916308	A7Vn	7.676	7.090	9.998	9.436	7.202	0.022	9.998	n	4	p
2MASS J08394575+1922011	G0	10.660	9.260	0.020	1.286	9.366	0.109	0.111	n	4	p
2MASS J08395072+1932269	K0III	6.590	4.390	0.040	130.702	4.348	0.015	0.043	n	7	p
2MASS J08395084+1933020	K	11.800	10.000	0.022	0.747	9.956	0.217	0.218	n	3,4	p
2MASS J08395234+1918455	F5V	10.230	9.010	0.020	1.846	8.973	0.080	0.083	n	4	p
2MASS J08395506+2003541	F4V	10.114	8.960	0.019	1.968	8.904	0.080	0.083	n	2,4	p
2MASS J08395649+1933107	Am	7.320	6.790	0.020	12.802	6.871	0.020	0.028	y	...	p
2MASS J08395777+1932293	Am	7.544	7.010	0.023	10.816	7.054	0.021	0.031	y	...	p
2MASS J08395807+1912058	F6V	9.488	8.480	0.018	3.166	8.388	0.050	0.053	n	4	p
2MASS J08395838+2009298	F2V	8.894	8.100	0.017	4.077	8.113	0.043	0.047	y	...	p
2MASS J08395908+2001532	F5V	9.233	8.210	0.021	3.659	8.230	0.040	0.045	y	...	p
2MASS J08395915+1940083	F3V	9.780	8.780	0.020	2.240	8.763	0.067	0.070	n	4	p
2MASS J08395957+1856357	A3	9.960	9.300	0.017	1.411	9.265	0.139	0.140	n	4	p
2MASS J08395983+1934003	K	11.920	9.480	0.018	1.251	9.396	0.117	0.119	n	4	p
2MASS J08395998+1934405	...	12.860	10.550	0.018	0.561	10.267	0.250	0.251	n	3,4	p
2MASS J08400062+1948235	F6V	10.300	9.080	0.020	1.776	9.015	0.091	0.094	n	4	p
2MASS J08400130+2008082	F6V	9.670	8.620	0.018	2.665	8.575	0.058	0.061	n	4	p
2MASS J08400171+1859595	F8V	10.020	8.700	0.018	2.704	8.559	0.072	0.074	n	4	p
2MASS J08400416+1947039	...	12.060	10.000	0.020	0.642	10.120	0.225	0.226	n	4	p
2MASS J08400491+1943452	F6V	9.790	8.650	0.020	2.572	8.613	0.060	0.063	n	4	p
2MASS J08400571+1901307	...	12.640	10.010	0.020	0.749	9.952	0.209	0.210	n	2,4	p
2MASS J08400627+1927148	F6V	10.240	8.870	0.020	2.048	8.861	0.075	0.077	n	4	p
2MASS J08400635+1918264	G8V	11.010	9.230	0.018	1.454	9.232	0.108	0.110	n	4	p
2MASS J08400643+2000280	G8III	6.390	4.200	0.027	154.238	4.168	0.015	0.031	n	77	p
2MASS J08400968+1937170	...	11.980	10.130	0.020	0.556	10.277	0.294	0.295	n	3,4	p
2MASS J08401145+1958161	A1V	6.610	6.530	0.023	16.269	6.610	0.019	0.030	y	...	p
2MASS J08401231+1938222	F5V	9.903	8.670	0.023	2.483	8.651	0.063	0.067	n	4	p
2MASS J08401345+1946436	...	13.190	10.640	0.020	...	...	...	...	n	3	p
2MASS J08401535+1959394	F2V	8.809	8.040	9.995	4.185	8.085	0.040	9.995	n	4	p
2MASS J08401549+1927310	K6V	13.920	10.690	0.020	...	...	...	...	n	3,4,6	p
2MASS J08401571+1954542	...	12.700	10.010	0.018	0.713	10.005	0.205	0.206	n	2,4	p
2MASS J08401762+1947152	F8V	9.960	8.580	0.018	2.486	8.650	0.063	0.066	n	4	p
2MASS J08401810+1931552	F0III	7.540	7.160	0.017	9.251	7.223	0.022	0.028	n	7	p
2MASS J08401893+2011307	K4V	12.970	10.040	0.018	0.958	9.685	0.156	0.157	n	3,4	p
2MASS J08402013+1920564	A9V	6.760	6.040	0.017	27.407	6.044	0.016	0.024	y	...	p
2MASS J08402075+1941120	F2III	7.680	7.280	0.023	8.416	7.326	0.023	0.032	n	7	p

Table 1
(Continued)

Name	Sp Type	V	K_S	$K_{\rm err}$	$f24$	[24]	$[24]_{\rm err}$	$(K–[24])_{\rm err}$	Incl?	Excl. Note	Cluster
2MASS J08402209+1940116	G9III	6.420	4.180	0.036	163.650	4.104	0.015	0.039	n	7	p
2MASS J08402231+2006243	F2III	10.057	8.850	0.018	2.249	8.759	0.064	0.067	n	1,4,7	p
2MASS J08402271+1927531	...	10.700	9.340	0.020	1.482	9.212	0.101	0.102	n	2,4	p
2MASS J08402327+1940236	F2	10.370	9.010	0.020	1.872	8.958	0.098	0.100	n	1,4	p
2MASS J08402347+1950059	F2III	8.025	7.590	0.020	6.641	7.583	0.027	0.034	n	7	p
2MASS J08402554+1928328	...	9.850	8.760	0.020	2.175	8.795	0.066	0.069	n	1,4	p
2MASS J08402614+1941111	F6V	9.361	8.370	0.018	3.376	8.318	0.047	0.050	n	4	p
2MASS J08402624+1913099	K3V	12.900	10.460	0.020	...	...	...	...	n	3,4,6	p
2MASS J08402675+2010552	F2Vn	8.203	7.430	0.020	7.688	7.424	0.025	0.032	y	...	p
2MASS J08402702+1932415	A5m	6.290	5.880	0.018	29.723	5.956	0.016	0.024	y	...	p
2MASS J08402743+1916409	G5V	11.170	9.650	0.020	1.027	9.610	0.149	0.151	n	2,4	p
2MASS J08402751+1939197	K4V	13.220	10.690	0.020	...	...	...	...	n	3	p
2MASS J08402863+2018449	K	11.640	9.460	0.018	1.134	9.502	0.198	0.199	n	2,4	p
2MASS J08403169+1951010	G9V	11.630	9.910	0.018	0.736	9.972	0.203	0.204	n	2,4	p
2MASS J08403184+2012060	G5V	11.520	9.830	0.014	0.782	9.906	0.181	0.182	n	3,4	p
2MASS J08403296+1911395	F0V	8.663	7.960	0.015	5.220	7.845	0.032	0.035	y	...	p
2MASS J08403347+1938009	...	12.209	10.170	0.018	...	...	...	...	n	3	p
2MASS J08403924+1913418	A9V	7.800	7.230	0.021	8.768	7.282	0.022	0.030	y	...	p
2MASS J08403992+1940092	G3V	10.870	9.190	0.018	1.409	9.267	0.098	0.100	n	4	p
2MASS J08404189+1913255	G1V	10.610	9.060	0.018	1.636	9.105	0.086	0.088	n	4	p
2MASS J08404248+1933576	G6V	11.340	9.710	0.018	1.028	9.608	0.140	0.141	n	2,4	p
2MASS J08404321+1943095	A9III	6.830	6.330	0.017	20.361	6.367	0.017	0.024	n	7	p
2MASS J08404608+1918346	F6V	9.562	8.530	0.020	2.838	8.506	0.052	0.056	n	2,4	p
2MASS J08404720+1932373	K3V	10.350	8.200	0.021	4.094	8.109	0.037	0.043	y	...	p
2MASS J08404798+1939321	G7V	11.020	9.250	0.018	1.399	9.274	0.103	0.105	n	2,4	p
2MASS J08404832+1955189	G3V	11.030	9.510	0.020	1.176	9.462	0.127	0.128	n	2,4	p
2MASS J08405247+2015594	F0Vn	8.478	7.800	0.018	5.328	7.822	0.039	0.043	y	...	p
2MASS J08405252+1928595	F7V	10.318	9.050	0.020	1.818	8.990	0.083	0.086	n	4	p
2MASS J08405487+1956067	K1V	12.090	10.130	0.018	0.625	10.150	0.240	0.241	n	2,4	p
2MASS J08405630+1934492	A6Vn	6.770	6.280	0.018	21.403	6.313	0.017	0.025	y	...	p
2MASS J08405669+1944052	...	12.230	10.210	0.020	0.594	10.203	0.263	0.264	n	3,4	p
2MASS J08405693+1956055	Am	8.713	8.050	0.023	4.497	8.006	0.034	0.041	y	...	p
2MASS J08410478+1931225	G5V:	11.040	8.750	0.020	2.428	8.676	0.064	0.067	n	4	p
2MASS J08410725+1926489	K1	12.430	10.290	0.018	0.631	10.139	0.328	0.329	n	3,4	p
2MASS J08410737+1904164	G0	10.180	8.640	0.019	...	...	...	...	n	3	p
2MASS J08410961+1951186	G	10.710	8.940	0.018	2.498	8.645	0.063	0.066	n	4	p
2MASS J08410979+1956072	...	13.630	10.760	0.020	...	...	...	...	n	3,4,6	p
2MASS J08411002+1930322	F6V	10.110	8.910	0.020	1.826	8.985	0.086	0.089	n	4	p
2MASS J08411031+1949071	...	11.520	9.750	0.020	0.954	9.690	0.145	0.146	n	2,4	p
2MASS J08411067+1949465	F5V	9.037	8.190	0.021	3.564	8.259	0.043	0.048	y	...	p
2MASS J08411319+1932349	...	...	10.350	0.018	0.642	10.120	0.255	0.256	n	3,4,5	p
2MASS J08411377+1955191	A5V	8.340	7.770	0.017	5.761	7.738	0.031	0.035	y	...	p
2MASS J08411541+2002160	...	14.290	11.020	0.018	...	...	...	...	n	3,4,6	p
2MASS J08411602+1944514	...	13.700	11.710	0.023	...	...	...	...	n	3,4,6	p
2MASS J08411840+1915394	A7Vn	7.914	7.290	0.023	10.539	7.082	0.021	0.031	y	...	p
2MASS J08411992+1938047	K5V	13.550	10.760	0.020	0.737	9.971	0.265	0.265	n	3,4	p
2MASS J08412258+1856020	K3V	12.960	10.540	0.019	...	...	...	...	n	3,4,6	p
2MASS J08412390+2014572	...	14.680	10.780	0.020	0.629	10.142	0.327	0.328	n	3,4	p
2MASS J08412584+1956369	A2	10.720	9.330	0.020	1.172	9.467	0.128	0.130	n	4	p
2MASS J08412698+1932329	F4V	9.880	8.720	0.020	2.081	8.843	0.071	0.074	n	4	p
2MASS J08412869+1944481	G1V	10.930	9.470	0.018	1.085	9.551	0.148	0.150	n	4	p
2MASS J08413384+1958087	...	11.710	9.930	0.018	0.734	9.975	0.205	0.206	n	3,4	p
2MASS J08413506+1939449	K0III	8.500	5.960	0.023	31.178	5.904	0.016	0.028	n	7	p
2MASS J08413599+1906255	...	14.170	10.980	0.018	...	...	...	...	n	3,4,6	p
2MASS J08413620+1908335	F4V	9.320	8.350	0.022	3.126	8.401	0.048	0.053	n	4	p
2MASS J08413741+1931140	K5V	13.570	10.730	0.018	0.522	10.345	0.296	0.297	n	3,4,6	p
2MASS J08414229+1939379	F6V	9.590	8.480	0.019	...	...	...	...	n	4,6	p
2MASS J08414368+1957437	...	12.360	10.260	0.019	0.599	10.194	0.373	0.374	n	3,4	p
2MASS J08414382+2013368	F7	10.470	9.140	0.018	1.828	8.984	0.107	0.109	n	4	p
2MASS J08414549+1916023	...	10.150	8.930	0.019	1.874	8.957	0.077	0.079	n	4	p
2MASS J08414776+1924439	...	11.420	10.100	0.021	0.704	10.019	0.219	0.220	n	2,4	p
2MASS J08414818+1927312	K5V	13.670	10.730	0.018	...	...	...	...	n	3	p
2MASS J08414934+1911471	K8V	14.500	10.830	0.018	...	...	...	...	n	3,4,6	p
2MASS J08415008+1952270	K0III	6.900	4.680	0.015	98.266	4.658	0.015	0.022	n	7	p
2MASS J08415199+2010013	...	12.040	10.090	0.019	0.773	9.918	0.221	0.222	n	3,4,6	p

Table 1
(Continued)

Name	Sp Type	V	K_S	$K_{\rm err}$	$f24$	[24]	$[24]_{\rm err}$	$(K–[24])_{\rm err}$	Incl?	Excl. Note	Cluster
2MASS J08415314+2009340	F2Vn	8.547	7.790	0.017	5.665	7.756	0.032	0.036	y	...	p
2MASS J08415437+1915266	G5V	11.410	9.640	0.019	0.964	9.679	0.149	0.150	n	2,4	p
2MASS J08415587+1941229	G5V	11.050	9.540	0.018	1.083	9.552	0.126	0.128	n	4	p
2MASS J08415782+1854422	F5V	9.426	8.430	0.025	2.923	8.474	0.076	0.080	n	4	p
2MASS J08415884+2006272	K4V	13.230	10.600	0.018	...	...	...	...	n	3,4,6	p
2MASS J08420547+1935585	K0	10.630	8.380	0.031	3.414	8.306	0.050	0.058	n	4	p
2MASS J08420650+1924405	A7V	7.954	7.430	0.024	7.589	7.438	0.024	0.034	y	...	p
2MASS J08421080+1856037	A7Vn	7.900	7.350	0.020	7.986	7.383	0.031	0.037	y	...	p
2MASS J08421149+1916373	...	12.150	10.170	0.016	...	...	...	...	n	4,6	p
2MASS J08421233+1912488	K6V	13.700	10.830	0.016	...	...	...	...	n	3	p
2MASS J08421285+1916040	K5V	13.500	10.480	0.014	0.663	10.086	0.213	0.213	n	2,4	p
2MASS J08421549+1941156	...	9.880	8.770	0.016	2.173	8.796	0.065	0.067	n	4	p
2MASS J08421883+2024350	...	12.420	10.190	0.019	...	...	...	...	n	3,4,6	p
2MASS J08422012+2002117	F6V	9.724	8.410	0.021	3.100	8.411	0.048	0.052	n	4	p
2MASS J08422162+2010539	F3Vn	9.226	8.280	0.021	3.836	8.179	0.043	0.048	y	...	p
2MASS J08422471+1935175	...	10.990	9.480	0.014	1.337	9.323	0.113	0.114	n	4	p
2MASS J08423225+1923463	...	10.990	9.460	0.016	1.224	9.419	0.125	0.126	n	4	p
2MASS J08424021+1907590	...	12.150	10.190	0.018	0.652	10.103	0.227	0.227	n	3,4	p
2MASS J08424071+1932354	F2III	9.770	8.720	0.018	2.453	8.665	0.063	0.066	n	2,4,7	p
2MASS J08424250+1905589	...	11.620	9.880	0.021	0.880	9.777	0.170	0.171	n	4	p
2MASS J08424372+1937234	...	12.120	9.800	0.020	1.092	9.543	0.132	0.134	n	2,4	p
2MASS J08424441+1934479	F6V	9.740	8.630	0.018	2.818	8.514	0.054	0.056	n	4	p
2MASS J08430055+2020161	G5V	11.440	9.770	0.020	1.017	9.621	0.222	0.223	n	2,4	p
2MASS J08430593+1926152	F8V	9.970	8.460	0.021	3.105	8.409	0.051	0.055	n	4	p
2MASS J08430822+1942475	K4V	13.330	10.670	0.017	...	...	...	...	n	3,4,6	p
2MASS J08431076+1931346	...	11.780	10.010	0.021	0.595	10.203	0.239	0.240	n	3,4	p
2MASS J08432019+1946086	...	10.770	9.360	0.018	1.392	9.280	0.111	0.112	n	4	p
2MASS J08433239+1944378	K0V:	12.330	10.220	0.022	0.801	9.879	0.191	0.192	n	4	p
2MASS J08433553+2011225	F6V	10.136	8.920	0.018	1.851	8.970	0.088	0.090	n	4	p
2MASS J08440734+2004369	...	10.150	9.060	0.018	1.750	9.031	0.119	0.120	n	4	p

Notes. The characteristics of all stars in our sample. A total of 355 are presented here. Notes for column for reason for exclusion are as follows: (1) contamination from nearby stars, (2) FWHM much greater or much less than 5.5 arcsec, (3) signal-to-noise ratio <3, (4) K–[24] error greater than 0.05, (5) no V mag, (6) no 24 μm counterpart within 1.″5 search radius, (7) giant stars.

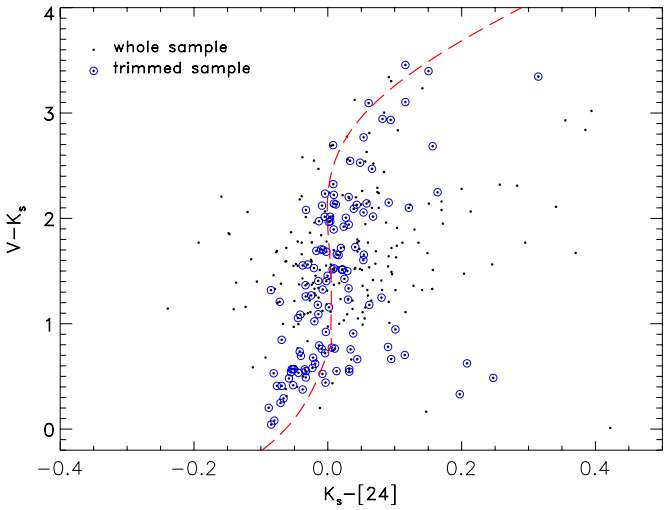

Figure 1. $V–K_S$ vs. K_S–[24] color–color plot for 670 Myr cluster members. The entire sample is shown as small dots, with circles indicating the ones retained in our analysis. The main-sequence locus presented in Equations (2) and (3) is shown as the dashed line.

(A color version of this figure is available in the online journal.)

Small color shifts in our clusters are possible due to effects such as metallicity differences or low levels of reddening (e.g., the probable reddening of Praesepe proposed by Taylor (2006) translates to ∼0.01 mag at K_S). We allowed the colors for each cluster to shift horizontally (in the K_S–[24] direction) to find the overall best fit to the ensemble of stars, with different shifts allowed for $x \leqslant 0$ and $x > 0$. We found the horizontal offset for each cluster by minimizing the calculated χ^2, defined as

$$\chi^2 = \sum[(K_S–[24])_{\rm observed} - (K_S–[24])_{\rm predicted}]^2. \quad (4)$$

We did not want to skew the χ^2 values with the redder K and M stars; therefore, we chose an upper bound of $V–K_S = 2.5$ for the χ^2 minimization. We included only a range between −0.1 and 0.1 in K_S–[24] (i.e., 3σ in our fit) so that possible excess stars did not contaminate our results. Table 2 gives shifted values for each of the clusters. We found a systematic offset of about 0.02 between the blue and red segments of the fit, which probably indicates a residual problem in our determination of the main-sequence locus. The scatter improves to 0.031 mag after implementing these shifts (Figure 2).

Table 2
Derived K_S–[24] Shifts in Each of the Clusters

Cluster	Stars with $V–K_S \leqslant 0.8$	Stars with $V–K_S > 0.8$
Hyades	+0.011	−0.009
Coma Ber	+0.028	+0.011
Praesepe	+0.009	−0.014

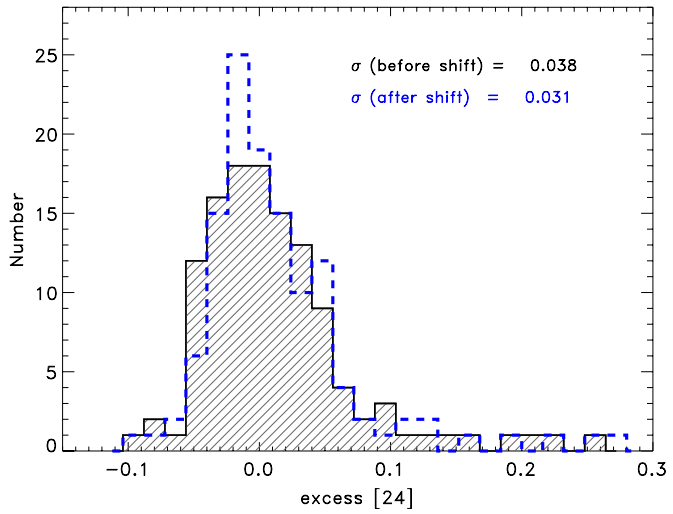

Figure 2. Histogram of V–[24] relative to the main-sequence locus, for the stars retained in our analysis. The general nature of the distribution is similar before and after we shift the loci for the individual clusters to minimize the deviations from it. The stars with excesses are shown by the low-lying distribution extending to positive values >0.1.

(A color version of this figure is available in the online journal.)

3. RESULTS

3.1. Identification of Stars with Excess Emission

We first identified excess candidates by requiring that the difference between the observed K_S–[24] and the predicted K_S–[24] is $\gtrsim$0.1 mag. There are nine stars that meet this criterion. To ensure that the excess is significant, we also compute χ_{24}, defined as

$$\chi_{24} = \frac{(K_S\text{–}[24])_{\rm observed} - (K_S\text{–}[24])_{\rm predicted}}{e_{K_S-[24]}}. \quad (5)$$

A significant excess requires $\chi_{24} \geqslant 3$ (Su et al. 2006; Trilling et al. 2008). One of the nine stars, 2MASS J08385506+1911539, from the Praesepe cluster failed this test ($\chi_{24} = 2.7$); we eliminated it from the list of confirmed excesses. We therefore find that 8 out of our sample of 122 stars have excesses at 24 μm greater than 10% of their photospheric emission and at a minimum 3σ confidence level (Figure 3 and Table 3). Five of these eight stars have previously been identified as having 24 μm excesses: HD 28226 and HD 28355 (Su et al. 2006; Cieza et al. 2008); 2MASS J08411840+1915394 (Gáspár et al. 2009); and HD 285690 and HD 286789 (Stauffer et al. 2010). The three stars with newly discovered excesses are HD 108382, HIP 21179, and 2MASS J08411840+1915394. Of these eight stars, five are from Hyades, two are from Praesepe, and one is from Coma Ber.

3.2. Comparison of Results from the Three Clusters

To first order, we have assumed that the data for all three clusters are homogeneous. This assumption can be tested by considering them individually. In addition to our overall $\sigma = 0.031$, we also calculate σ for each individual cluster, applying a Gaussian fit to the data in each cluster separately. We exclude stars that are >+3σ from the photospheric locus using the original σ value and obtain a new σ value for each cluster. Given the small number of sources in the individual clusters, the differences in the scatter around the main-sequence locus (see Figure 3) are not very significant. Nonetheless, we tested if the individual values would change any of our results. For Hyades we find $\sigma = 0.027$; however, adopting this value does not allow us to identify any new excess sources. For Coma Ber we find $\sigma = 0.036$, which is larger than the original value. However, the only source from Coma Ber with excess still remains beyond this new 3σ threshold. Finally, for Praesepe we find $\sigma = 0.032$, which is similar to the overall average for the three clusters. We suspect that the differences in σ are due to small number statistics, but in any case they do not affect our conclusions.

3.3. Possible False Detections

A general possibility for false detections is confusion with background infrared-emitting galaxies. For this situation, we have adapted the analysis of Gáspár et al. (2009), adjusting for our smaller matching radius (1.″5 versus 3.″6). Because faint and distant galaxies are uniformly distributed over the sky, the analysis should apply to all three clusters. We find that there is a 10% probability of a single chance coincidence in our entire sample and a 5% probability of two coincidences. We therefore make no corrections for such matches.

Plavchan et al. (2009) discuss the possibility that an M dwarf spectroscopic binary companion to a K dwarf may produce 10% "excess" (superphotospheric) flux at 24 μm. This would produce an artificial excess (false positive) source in our color–color space. There is only one known binary K star in our sample that shows an excess: HIP 21179 (Bender & Simon 2008). This star is considered to be a secure member of the Hyades (Perryman et al. 1998) with a relatively high X-ray luminosity (Stern et al. 1995). The masses of the components are 0.79 ± 0.08 $M_\odot$ and 0.58 ± 0.15 $M_\odot$ (Bender & Simon 2008). It is variable (V1147 Tau) with an amplitude in the visible of ~0.17 mag (Watson et al. 2011). The HIP 21179 excess is 6σ and 19% higher than the photospheric prediction, but given this list of issues we do not consider the presence of a debris disk to be secure and discard it from our sample of disks.

The second late-type star with an apparent excess is HD 285690. It is also a secure Hyades member (Perryman et al. 1998) but has no evidence for binarity and is of low X-ray luminosity (Stern et al. 1995). Although it is variable (V985 Tau), the amplitude is only 0.02 mag (Watson et al. 2011), not at a level that significantly undermines the identification of the 24 μm excess. This star is therefore likely to be a genuine debris disk detection. The third such star, HD 286789, is also a secure Hyades member with low X-ray luminosity. It shows variability of 0.06 mag in the visible (Watson et al. 2011), but given the general reduction in variability amplitude for late dwarf stars in the infrared (e.g., Koen et al. 2005), the excess is reasonably secure. Since the χ^2 value for the excess of HD 286789 is only slightly above 3, we combined the 2MASS H and K measurements (the error on J is large) to compute an equivalent K of 7.792 ± 0.022 and a new χ^2 of 3.7. Both of these stars are sufficiently bright at 24 μm that the probability of chance coincidences with background galaxies that might create false excesses is small: ~1% for one or more such coincidences in our entire sample (scaling from Gáspár et al. 2009). We therefore retain both stars in our sample.

3.4. Comparison to Previous Work

Our work is the first analysis of the *Spitzer* MIPS data for Coma Ber; however, the observations of the Hyades have been analyzed previously by Cieza et al. (2008) and Stauffer et al. (2010), while a paper on Praesepe has been published by Gáspár

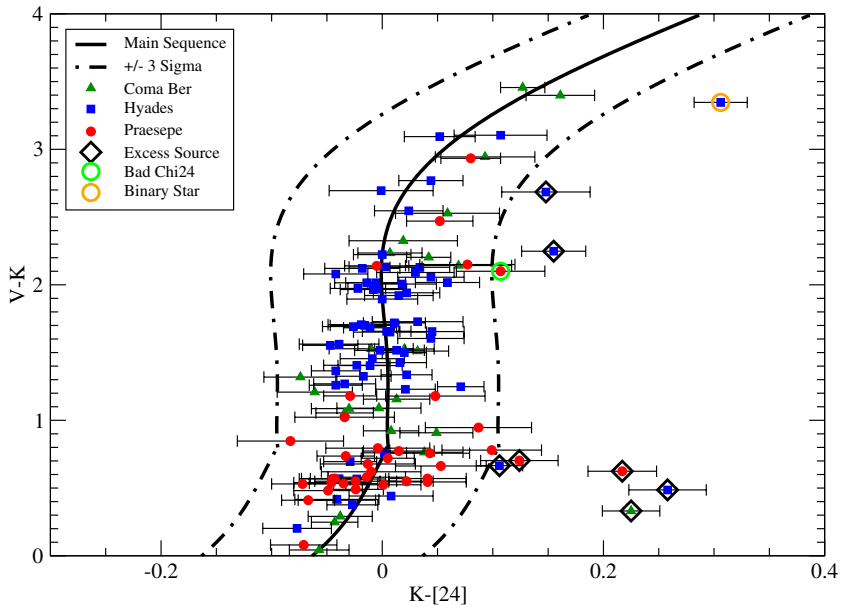

Figure 3. $V-K_S$ vs. K_S–[24] color–color plot for 670 Myr cluster members that we retain in our analysis. The solid line is the locus of main-sequence stars and the dash-dot lines are at 3σ above and below in K_S–[24]. The stars that pass our tests for having 24 μm excesses are indicated with diamonds. One additional star circled in green, 2MASS J08385506+1911539, lies to the right of the 3σ locus but fails our signal-to-noise criterion for a verified excess, as can also be seen by the large error bars for it (Section 3.1). HIP 21179 is circled in orange because of a possible false excess due to a binary companion (Section 3.3).

(A color version of this figure is available in the online journal.)

Table 3
Identified 24 μm Excess Sources

Name	Type	Excess[a]	Error[b]	χ_{24}	Cluster	Previous ID
HD 028226	Am	0.109	0.021	5.2	Hyades	Su et al. (2006)
HD 028355	A7V	0.273	0.035	7.9	Hyades	Su et al. (2006)
HD 285690	K0	0.155	0.029	5.3	Hyades	Stauffer et al. (2010)
HD 286789	K7	0.127	0.040	3.7	Hyades	Stauffer et al. (2010)
HIP 21179	K0	0.188	0.024	7.7	Hyades	None[c]
HD 108382	A4V	0.252	0.026	9.5	Coma Ber	None
2MASS J08385506+1911539	K3V	0.108	0.040	2.7	Praesepe	None[d]
2MASS J08403296+1911395	F0V	0.125	0.035	3.6	Praesepe	None
2MASS J08411840+1915394	A7V	0.223	0.031	7.2	Praesepe	Gáspár et al. (2009)
HD 026784	F8V	0.094	0.017	5.5	Hyades	Stauffer et al. (2010)[e]
2MASS 08410961+1951186	G	0.309	0.066	4.7	Praesepe	Gáspár et al. (2009)[e]
Melotte 111 AV 573	~K0	0.21	0.057	3.8	Coma Ber	None[e]

Notes.
[a] $(K_S\text{–}[24])_{\rm observed} - (K_S\text{–}[24])_{\rm predicted}$, in magnitudes.
[b] Error calculated using Equation (1).
[c] Excess probably not associated with a debris disk; see Section 3.3.
[d] Fails χ_{24} test, see Section 3.1.
[e] Secondary sample; see Sections 3.4 and 3.5.

et al. (2009). In the Hyades, Cieza et al. (2008) found only a single star with a significant excess, HD 28355; this star is also found to have an excess by Su et al. (2006) and in our work. The identification of five additional stars with excesses by Stauffer et al. (2010) and by us results directly from the smaller rms scatter in the data reduction and our more accurate extrapolation of the photospheric emission to 24 μm. Stauffer et al. (2010) found an excess for one case not in our sample, the F8V star, HD 26784. We agree that it has a nominal excess of ~0.09 mag ($K_S = 5.862$, [24] = 5.782, shift of −0.014), near the threshold for detection, but it fell below our uniform threshold for an excess of 0.1 mag. The largest term in the uncertainty for this star is the 2MASS K magnitude. We have augmented it by using standard *JHK* colors (Tokunaga 2000; Carpenter et al. 2008, with the correction described in Rieke et al. 2008) appropriate for its $V - K$ color (=1.26) to compute equivalent K magnitudes from 2MASS J and H, assuming an additional uncertainty of 0.01 for $J - K$ and 0.005 for $H - K$. A weighted average of the three measures yields $K = 5.862 \pm 0.012$, and confirms that an excess is detected for this star at a statistically significant level.

Gáspár et al. (2009) identified four stars with probable excesses in Praesepe; three of them (numbers 77, 134, and 181) do not pass the signal-to-noise threshold for inclusion in our sample. The remaining star, number 143 = 2MASS J08411840+1915394, is also found to have an excess in our study, while our measurement of number 134 = 2MASS J08410961+1951186 verifies its excess, even if its error

in K_S–[24] was too large to include it in our sample. The remaining two sources, numbers 77 = 2MASS J08395998+1934405 and 181 = 2MASS J08424021+1907590, do not pass our criteria for firmly established excesses because our noise estimation is significantly more conservative (larger noise) than that used by Gáspár et al. (2009).

3.5. Secondary Sample

The case of HD 26784 suggests that there may be other plausible excesses below our overall threshold of K_S–[24] > 0.1 and [24] error $\leqslant$ 0.05. In fact, a search relaxing the requirements on size of excess and K_S–[24] error yields Melotte 111 AV 573 = 2MASS J12133585+2910216 from Coma Ber as having evidence for a debris disk.

We divide the detected excesses into two samples. The primary one is defined by our initial criteria (excess at $>3\sigma$ significance and >0.1 mag) and can be compared directly with previous studies identifying excesses by similar criteria. The secondary sample consists of HD 26784 (F8V), Melotte 111 AV 573 (∼K0), and 2MASS J08410961+1951186 (∼G4 from its $V-K$ color).

4. DISCUSSION

From our study, the overall rate of 24 μm excesses >10% of the photospheric level at 670 Myr is $5.7^{+3.1}_{-1.7}$% (7/122 sources). The errors (here and in the following) are calculated using a binomial distribution for small number statistics. Our result is higher than the excess rate for Praesepe of $2.1^{+4.1}_{-2.1}$% (4/193 sources) found by Gáspár et al. (2009), but the difference can be largely explained by the smaller threshold for identifying an excess in our study (0.1 mag instead of 0.15); in any case, the two values agree within the errors.

We now compare the evolution as a function of stellar type. A first-order estimate of the timescale for debris disk evolution is given by Wyatt (2008), Equation (16). To apply this result, we assume an average luminosity ratio of 8 between our early-type (B9–F4) and solar-like (F5–K9) samples and a mass ratio of 1.7. The thermal equilibrium distance from the fiducial stars is then different by a factor of 2.8. We assume that typical planetesimal disk masses scale with the mass of the star (Natta et al. 2000). We find that the timescale is dominated by the strong radial dependence in Equation (16), which indicates that the decay around the early-type stars should be an order of magnitude slower than around the solar-like ones.

Our sample is ideally suited to determine the excess rate for stars near the mass of the Sun and with well-constrained ages near 670 Myr. We used spectral types from SIMBAD and placed stars without a given spectral type from SIMBAD in bins according to their $V-K_S$ colors using Table 3 in Koornneef (1983). We find that the excess rate for F5–K9 type stars is $2.7^{+3.3}_{-1.7}$% (2/75 stars), in agreement with the value of 1.9% ± 1.2% from Gáspár et al. (2009). However, the secondary sample includes three well-detected debris disks around stars in the same spectral range, so this value may be a modest underestimate. We can compare it with that obtained by Sierchio et al. (2010), who measured the excess rate for stars in the same spectral range in the 115 Myr Pleiades cluster and the similar-age Blanco 1 association using the same reduction method and excess threshold of 10%. They report an excess rate of $31.5^{+5.2}_{-4.5}$% at 24 μm (28/89). We can add to their sample observations in the α Per cluster (Carpenter et al. 2009) at an age of 85 Myr, for a total of $29.4^{+4.9}_{-4.1}$% (30/102) at an age of ∼100 Myr.

We have assembled similar data for B9–F4 stars from the literature. For the age range 50–99 Myr there are 17/47 stars with 24 μm excesses, or $36.2^{+7.3}_{-6.2}$% (Rieke et al. 2005; Su et al. 2006; Siegler et al. 2007; Balog et al. 2009), while in the 100–199 Myr range there are 33/93, or $35.5^{+5.1}_{-4.6}$% (Rieke et al. 2005; Su et al. 2006; Gorlova et al. 2006). The combined result for 50–199 Myr is $35.7^{+4.3}_{-3.8}$% (50/140). In the 400–1000 Myr range, the corresponding number is 6/77, or $7.8^{+4.2}_{-2.1}$% (Su et al. 2006; this work). This value agrees well with that in Gáspár et al. (2009) of 6.5% ± 4.1%.

The incidence of debris disks at ∼100 Myr shows no difference between the two ranges of spectral type. At ∼670 Myr, the later spectral types show a lower incidence, but the two values still agree at the 1.5σ level. Moreover, the detection of three later-type stars in the secondary sample (of which HD 26784 only barely misses the primary sample) suggests that a significant number of such stars retain debris disks at this age. This conclusion has been reached previously (e.g., Trilling et al. 2008; Gáspár et al. 2009; Carpenter et al. 2009).

However, all previous such works have depended in part or entirely on samples of field stars. Given the uncertainties in age estimates for these stars, combined with the rapid decline in the incidence of excesses (from ∼30% at 100 Myr to ∼3% at 670 Myr), age errors that place a small number of young stars among the older part of a sample could yield the observed number of excesses. Our work removes this source of uncertainty by basing the result entirely on observations of cluster members with well-determined ages. Thus, the data appear to contradict the first-order theoretical timescale difference for disk decay as a function of stellar type.

5. CONCLUSION

We used 24 μm *Spitzer* observations of stars in three clusters (Hyades, Coma Ber, and Praesepe) to measure the incidence of debris disks at ∼670 Myr and over a broad range of spectral types. The combination of three clusters at the same age gives a better representation of the excess behavior because we can use the closest cluster (Hyades) to detect excesses around low-mass stars, while having access to significant numbers of higher mass stars in the more distant cluster (Praesepe). We compared the $V-K_S$, K_S–[24] of the cluster members with the color locus of 1300 field stars. The dispersion around this locus is 10% (3σ), which we adopt as the threshold for identification of an excess.

We find an overall excess rate of $5.7^{+3.1}_{-1.7}$% for stars at ∼670 Myr. This value shows substantial decay from the rates of $29.4^{+4.9}_{-4.1}$% for F5–K9 stars and $35.7^{+4.3}_{-3.8}$% for B9–F4 stars at ∼100 Myr. However, the decay appears to be similar within the errors between these ranges of spectral types. This result is contrary to first-order estimates, which would indicate an order-of-magnitude slower decay for the early-type stars than the solar-like ones.

This work was supported at Northern Arizona University by funding from the Spitzer Science Center/JPL. Funding was also provided by the National Science Foundation through a Research Experience for Undergraduates (REU) position at Northern Arizona University. Support was also provided by contract 1255094 from Caltech/JPL to the University of Arizona. This research made use of the SIMBAD and Vizier database, operated at CDS, Strasbourg, France. This work also uses data products from the Two Micron All Sky Survey, which is a joint project of the University of Massachusetts

and the Infrared Processing and Analysis Center/California Institute of Technology, funded by the National Aeronautics and Space Administration and the National Science Foundation. We also thank Jennifer Sierchio and Andras Gáspár for helpful comments and discussions and the anonymous referee, whose suggestions improved this paper.

REFERENCES

Abad, C., & Vicente, B. 1999, VizieR Online Data Catalog, 413, 60307
Agnor, C. B., Canup, R. M., & Levison, H. F. 1999, Icarus, 142, 219
Aumann, H. H., Beichman, C. A., Gillett, F. C., et al. 1984, ApJ, 278, L23
Balog, Z., Kiss, L. L., Vinkó, J., et al. 2009, ApJ, 698, 1989
Bender, C. F., & Simon, M. 2008, ApJ, 689, 416
Carpenter, J. M., Bouwman, J., Mamajek, E. E., et al. 2009, ApJS, 181, 197
Carpenter, J. M., Bouwman, J., Silverstone, M. D., et al. 2008, ApJS, 179, 423
Chambers, J. E. 2001, Icarus, 152, 205
Cieza, L. A., Cochran, W. D., & Augereau, J.-C. 2008, ApJ, 679, 720
Collier, C. A., Davidson, V. A., Hebb, L., et al. 2009, MNRAS, 400, 451
Cutri, R. M., Skrutskie, M. F., van Dyk, S., et al. 2003, The IRSA 2MASS All-Sky Point Source Catalog, NASA/IPAC
Decin, G., Dominik, C., Malfait, K., Mayor, M., & Waelkens, C. 2000, A&A, 357, 533
Decin, G., Dominik, C., Waters, L. B. F. M., & Waelkens, C. 2003, ApJ, 598, 636
De Gennaro, S., von Hippel, T., Jeffreys, W. H., et al. 2009, ApJ, 696, 12
Dominik, C., & Decin, G. 2003, ApJ, 598, 626
Engelbracht, C. M., Blaylock, M., Su, K. Y. L., et al. 2007, PASP, 119, 994
Gáspár, A., Rieke, G. H., Su, K. Y. L., et al. 2009, ApJ, 697, 1578
Gomes, R. S., Morbidelli, A., & Levison, H. F. 2004, Icarus, 170, 492
Gordon, K. D., Rieke, G. H., Engelbracht, C. W., et al. 2005, PASP, 117, 503
Gorlova, N., Rieke, G. H., Muzerolle, J., et al. 2006, ApJ, 649, 1028
Habing, H. J., Dominik, C., Jourdain de Muizon, M., et al. 2001, A&A, 365, 545
Hahn, J. M., & Malhotra, R. 1999, AJ, 117, 3041
Haisch, K. E., Jr., Lada, E. A., & Lada, C. J. 2001, ApJ, 553, L153
Kenyon, S. J., & Bromley, B. C. 2004, ApJ, 602, 133
Koen, C., Tanabé, T., Tamura, M., & Kusakabe, N. 2005, MNRAS, 362, 727
Koerner, D. W., Kim, S., Trilling, D. E., et al. 2010, ApJ, 710, L26
Koornneef, J. 1983, A&AS, 51, 489
Lagrange, A.-M., Backman, D. E., & Artymowicz, P. 2000, in Protostars and Planets IV, ed. V. Mannings, A. P. Boss, & S. S. Russell (Tucson, AZ: Univ. Arizona Press), 639
Levison, H. F., Morbidelli, A., Gomes, R., & Backman, D. 2007, in Protostars and Planets V, ed. B. Reipurth, D. Jewitt, & K. Keil (Tucson, AZ: Univ. Arizona Press), 669
Meyer, M. R., Carpenter, J. M., Mamajek, E. E., et al. 2008, ApJ, 673, L181
Morales, F. Y., Rieke, G. H., Werner, M. W., et al. 2011, ApJ, 730, L29
Morishima, R., Stadel, J., & Moore, B. 2010, Icarus, 207, 517
Natta, A., Grinin, V., & Mannings, V. 2000, in Protostars & Planets IV, ed. V. Mannings, A. P. Boss, & S. S. Russell (Tucson, AZ: Univ. Arizona Press), 559
Paulson, D. B., Cochran, W. D., & Hatzes, A. P. 2004, AJ, 127, 3579
Perryman, M. A. C., Brown, A. G. A., Lebreton, Y., et al. 1998, A&A, 331, 81
Perryman, M. A. C., Lindegren, L., Kovalevsky, J., et al. 1997, A&A, 323, L49
Plavchan, P., Werner, M. W., Chen, C. H., et al. 2009, ApJ, 698, 1068
Raymond, S. N., Quinn, T., & Lunine, J. I. 2006, Icarus, 183, 265
Rhee, J. H., Song, I., Zuckerman, B., & McElwain, M. 2007, ApJ, 660, 1556
Rieke, G. H., Blaylock, M., Decin, L., et al. 2008, AJ, 135, 2245
Rieke, G. H., Su, K. Y. L., Stansberry, J. A., et al. 2005, ApJ, 620, 1010
Rieke, G. H., Young, E. T., Engelbracht, C. W., et al. 2004, ApJS, 154, 25
Siegler, N., Muzerolle, J., Young, E. T., et al. 2007, ApJ, 654, 580
Sierchio, J. M., Rieke, G. H., Su, K. Y. L., et al. 2010, ApJ, 712, 1421
Spangler, C., Sargent, A. I., Silverstone, M. D., Becklin, E. E., & Zuckerman, B. 2001, ApJ, 555, 932
Stauffer, J. R., Rebull, L. M., James, D., et al. 2010, ApJ, 719, 1859
Stern, R. A., Schmitt, J. H. M. M., & Kahabka, P. T. 1995, ApJ, 448, 683
Su, K. Y. L., Rieke, G. H., Stansberry, J. A., et al. 2006, ApJ, 653, 675
Su, K. Y. L., Rieke, G., Stapelfeldt, K., et al. 2010, BAAS, 42, 349
Taylor, B. J. 2006, AJ, 132, 2453
Tokunaga, A. T. 2000, in Allen's Astrophysical Quantities, ed. A. N. Cox (4th ed.; New York: AIP Press), 143
Trilling, D. E., Bryden, G., Beichman, C. A., et al. 2008, ApJ, 674, 1086
Watson, C., Henden, A. A., & Price, A. 2011, AAVSO Variable Star Index (online at VizieR)
Wyatt, M. C. 2008, ARA&A, 46, 339